Journal of Engineering Physics and Thermophysics, Vol. 82, No. 5, 2009

NON-DARCIAN CONVECTION FLOW IN A CIRCULAR DUCT PARTIALLY FILLED WITH POROUS MEDIUM

D. V. Krishna

UDC 536.25

The flow and heat transfer in a circular duct bounded by a porous bed is considered. The entire flow region is divided into two zones. The clean fluid region is described by the Navier–Stokes equations, while the Brinkman-extended Darcy model is used in the flow through a porous bed. In either zone the momentum and temperature equations are coupled. In order to obtain a better insight into this complex problem, the Galerkin finite element analysis with quadratic polynomial approximations is applied. The behavior of the velocity and temperature is analyzed. The shear stress and the rate of heat transfer are also obtained for various governing parameters.

Keywords*: Non-Darcy convection; heat transfer; circular duct; porous bed; Galerkin finite element analysis.*

Introduction. Convective heat transfer in channels partially filled with porous media has gained considerable attention in recent years because of its various applications in contemporary technology. These applications include porous journal bearing, nuclear reactors, porous flat plate collectors, packed bed thermal storage, solidification of concentrated alloys, fibrous and granular insulations, grain storage and drying, paper drying, and food storage. Moreover, porous substrates, which are considered as composites of fluid and porous layers to improve forced convection heat transfer in channels, find applications in heat exchangers, chemical reactors, etc. With the use of the simple Darcy model, the fluid mechanics at the interface between a fluid layer and a porous medium over a flat plate has been first investigated by Beavers and Joseph [1]. Later, this problem was studied analytically by Vafai and Thiyagaraja [2], who obtained an approximate solution based on matched asymptotic expansions for the velocity and temperature distributions. Vafai and Kim [3] presented an exact solution for the same problem. Excluding the microscopic inertial term, closed-form analytical solutions for parallel plates and circular pipes partially filled with porous materials were obtained by Poulikakos and Kazmierczak [4] for a constant wall heat flux, while numerical results were computed for constant wall temperature. Jang and Chen [5] investigated numerically the problem of forced convection in a parallel plate channel partially filled with a porous material. They used the Darcy–Brinkman–Forchheimer model for the flow within a porous material. Vafai and Kim [6] studied the interaction between a porous medium and a clean fluid with the use of the Darcy–Brinkman–Forchheimer model and the continuity of velocities and stresses at the interface and discussed the effects of several parameters, such as the porous layer thickness, system configuration, Forchheimer coefficient, and the Darcy number. The study included the effects of these parameters on the transient thermal behavior of the channel under consideration.

Keeping the foregoing in view, we will consider the flow and heat transfer in a circular duct bounded by a porous bed. The entire flow region is divided into two zones: zone 1 consisting of a clean fluid and zone 2 — of a porous bed. In order to obtain a better insight into the problem, we will use the Galerkin finite element analysis with quadratic polynomial approximations.

Formulation of the Problem. We consider a free and forced convection flow in a vertical circular cylinder with a flowing clean fluid (zone 1) bounded by a coaxial porous matrix (zone 2) abutting the rigid cylindrical wall that is maintained at a constant temperature. The flow and temperature in the clean fluid and porous regions are assumed to be fully developed. Both the fluid and porous regions have constant physical properties, and a mixed convection flow takes place under the conditions of thermal buoyancy and uniform axial pressure gradient. The Boussinesq approximation is invoked, so that the density variation is confined to the thermal buoyancy force. The flow in the clean fluid region is governed by the Navier–Stokes equations, while the Brinkman–Forchhimer–extended Darcy

Department of Mathematics, Shirdi Sai Engineering College, Anekal, Bangalore, India. Published in Inzhenerno-Fizicheskii Zhurnal, Vol. 82, No. 5, pp. 879–885, September–October, 2009. Original article submitted May 22, 2008.

model that accounts for the inertia and boundary effects is used for the momentum equation in the porous region. In both zones the momentum and energy equations are coupled and, in particular, the equations in the porous region are nonlinear coupled ones. Moreover, the flow in either zone is unidirectional along the axial direction of the cylinder. On the basis of the above assumptions, the governing equations (respectively equations of linear momentum, energy, and state) for the clean fluid region are

$$-\frac{\partial p}{\partial z}+\mu\left(\frac{\partial^2 u}{\partial r^2}+\frac{1}{r}\frac{\partial u}{\partial r}\right)-\rho g=0\,, \tag{1}$$

$$\rho c_p u\frac{\partial T}{\partial z}=\lambda\left(\frac{\partial^2 T}{\partial r^2}+\frac{1}{r}\frac{\partial T}{\partial r}\right), \tag{2}$$

$$\rho-\rho_0=-\beta\rho_0\,(T-T_0)\,. \tag{3}$$

The corresponding equations in the porous region are

$$-\frac{\partial p}{\partial z}+\frac{\mu}{\delta}\left(\frac{\partial^2 u_{\rm p}}{\partial r^2}+\frac{1}{r}\frac{\partial u_{\rm p}}{\partial r}\right)-\frac{\mu}{k}u_{\rm p}-\frac{\rho\delta F}{\sqrt{k}}u_{\rm p}^2+\rho g\beta\,(T_{\rm p}-T_0)=0\,, \tag{4}$$

$$\rho c_p u_{\rm p}\frac{\partial T_{\rm p}}{\partial z}=\lambda\left(\frac{\partial^2 T_{\rm p}}{\partial r^2}+\frac{1}{r}\frac{\partial T_{\rm p}}{\partial r}\right), \tag{5}$$

where F is the function that depends on the Reynolds number and microstructure of the porous medium.

In zone 1 the symmetric conditions take place due to the symmetry with reference to the axis of the circular duct:

$$\frac{\partial u}{\partial r}=0\,,\quad \frac{\partial T}{\partial r}=0\quad\text{at}\quad r=0\,. \tag{6}$$

The boundary conditions for zone 2 are

$$u=0\,,\quad T=T_1\quad\text{at}\quad r=a+s\,. \tag{7}$$

In addition to the above, the following matching conditions hold at the fluid–porous bed interface $r = a$:

$$u=u_{\rm p}\,,\quad \frac{\partial u}{\partial r}=\frac{\partial u_{\rm p}}{\partial r}\,; \tag{8}$$

$$T=T_{\rm p}\,,\quad \frac{\partial T}{\partial r}=\frac{\partial T_{\rm p}}{\partial r}\,. \tag{9}$$

Conditions (8) correspond to the continuity of the velocity and shear stress at the interface, whereas (9) — to the continuity of the temperature and heat flux.

Introducing the suitable nondimensional variables into the governing equations, we obtain the following nondimensional equations (without any indices for nondimensional quantities):
for zone 1 ($0 \le r \le 1$)

$$\frac{d^2u}{dr^2} + \frac{1}{r}\frac{du}{dr} = P - \mathrm{G}\theta\,, \tag{10}$$

$$\frac{d^2\theta}{dr^2} + \frac{1}{r}\frac{d\theta}{dr} = \mathrm{Pr\,Nu}\,; \tag{11}$$

for zone 2 ($1 \le r \le 1 + s$)

$$\frac{d^2u_\mathrm{p}}{dr^2} + \frac{1}{r}\frac{du_\mathrm{p}}{dr} = P + \delta D^{-1} + \delta^2\Lambda u_\mathrm{p}^2 - \delta\mathrm{G}\theta_\mathrm{p}\,, \tag{12}$$

$$\frac{d^2\theta_\mathrm{p}}{dr^2} + \frac{1}{r}\frac{d\theta_\mathrm{p}}{dr} = \mathrm{Pr\,Nu_p}\,, \tag{13}$$

where

$$\Lambda = FD^{-1}\,,\quad \mathrm{G} = \frac{g\beta\,(T_1 - T_0)\,a^3}{\gamma^2}\,,\quad D^{-1} = \frac{a^2}{k}\,,\quad N = \frac{Aa}{T_1 - T_0}\,,\quad \mathrm{Pr} = \frac{\rho c_p \gamma}{\lambda}\,,\quad P = \frac{ga^3}{\gamma^2}\,.$$

The corresponding nondimensional conditions look like

$$\frac{du}{dr} = 0\,,\quad \frac{d\theta}{dr} = 0 \quad \text{at} \quad r = 0\,; \tag{14}$$

$$u_\mathrm{p} = 0\,,\quad \theta_\mathrm{p} = 1 \quad \text{at} \quad r = 1 + s\,, \tag{15}$$

and the interfacial conditions are

$$u = u_\mathrm{p}\,,\quad \frac{du}{dr} = \frac{du_\mathrm{p}}{dr} \quad \text{at} \quad r = 1\,; \tag{16}$$

$$\theta = \theta_\mathrm{p}\,,\quad \frac{d\theta}{dr} = \frac{d\theta_\mathrm{p}}{dr} \quad \text{at} \quad r = 1 + s\,. \tag{17}$$

Finite Element Analysis. The finite element analysis with quadratic polynomial approximation functions is carried out along the radial distance across the circular duct. The profiles of the velocity and temperature are obtained for different values of the governing parameters. The Galerkin method is adopted in variational formulation in each element of both zones to obtain the global coupled matrices for the velocity and temperature in the course of the finite element analysis. This method has two important features. Firstly, the approximation solution is written directly as a linear combination of approximation functions with unknown nodal values as coefficients. Secondly, the approximation polynomials are chosen exclusively from the lower order piecewise polynomials restricted to contiguous elements. Solving the ultimate coupled global matrix equations for the temperature and velocity and using the iteration procedure, we determine the unknown global nodes through which the temperature and velocity within different radial intervals are obtained. The expressions for the velocities are given as

$$u\,(r) = 50\left(-\frac{n}{5} + r\right)\left(-\frac{2n-1}{10} + r\right)u_{2n-1} - 100\left(-\frac{n}{5} + r\right)\left(-\frac{n-1}{5} + r\right)u_{2n}$$

$$+ 50\left(-\frac{2n-1}{10}+r\right)\left(-\frac{n-1}{5}+r\right)u_{2n+1}\,,$$

$$0.2\,(n-1) \le r \le 0.2n\,, \quad n = 1, 2, 3, 4, 5\,;$$

$$u_{\mathrm{p}}\,(r) = \frac{1}{s^2}\left\{50\left(-1+r-\frac{ns}{5}\right)\left[-1+r-\frac{(2n-1)\,s}{10}\right]u_{\mathrm{p},9+2n} - 100\left(-1+r-\frac{ns}{5}\right)\right.$$

$$\left.\times\left[-1+r-\frac{(n-1)\,s}{5}\right]u_{\mathrm{p},10+2n} + 50\left[-1+r-\frac{(2n-1)\,s}{10}\right]\left[-1+r-\frac{(n-1)\,s}{5}\right]u_{\mathrm{p},11+2n}\right\},$$

$$1 + 0.2s\,(n-1) \le r \le 1 + 0.2sn\,.$$

The same expressions are valid for the temperatures $\theta(r)$ and $\theta_{\mathrm{p}}(r)$.

The shear stress on the cylinder is evaluated using the formula

$$\tau = \left(\frac{du}{dr}\right)_{r=1+s}\,.$$

The rate of heat transfer (Nusselt number) on the cylinder is expressed as

$$\mathrm{Nu} = -\left(\frac{d\theta}{dr}\right)_{r=1+s}\,.$$

Results and Discussion. The velocity and temperature profiles, as well as the shear stress and Nusselt number, are evaluated for various governing parameters D^{-1}, G, and s. The influence of the thickness of the porous bed on the velocity and temperature in the bed and clean fluid regions and on the rate of heat transfer is also investigated. For all the cases considered the following values of parameters are used: P = 1, Pr = 7, N = 0.5.

The velocity gradually reduces in magnitude from its maximum on the axis of the duct to zero on the outer boundary in accordance with the non-slip condition. We may note that the thickness of the porous bed significantly affects the velocity and temperature in both regions. In fact, for a sufficiently large thermal buoyancy parameter ($\mathrm{G} \ge 10^2$), when the thickness of the porous bed increases, the magnitude of the velocity and temperature steeply rises in both the clean fluid and porous regions. The actual axial velocity is vertically downward in view of the imposed pressure gradient chosen to be positive. Any upward flow corresponds to a reversal flow.

Figures 1a and 2a show the profiles of the velocity for different values of G and D^{-1}, respectively, when the thickness of the porous bed is small. Figures 1b and 2b present these profiles for larger thickness of the porous bed. From Fig. 1a we notice that when s is small, an increase in the thermal buoyancy parameter G gradually reduces the axial velocity in both the clean fluid and porous regions. It follows from Fig. 2a that an increase in D^{-1} also reduces the velocity in the clean fluid, but slightly enhances it in the porous bed. Thus, as the permeability of the thin porous bed is reduced, the fluid in the clean region moves with a lower velocity. For large values of s, when G increases, the velocity changes the direction, its magnitude steeply rises, and the higher the value of G, the greater is the velocity (Fig. 1b). We find also that the velocity profiles are asymmetric parabolic with a maximum attained at r = 0.4. Figure 2b corresponds to the velocity profiles for different values of D^{-1}. We can see that, when D^{-1} rises, the velocity first increases, then decreases, and further again sharply increases.

The behavior of the nondimensional temperature for different thicknesses of the porous bed may be observed in Figs. 3 and 4. In the case of a thin porous bed, as G rises, the temperature increases in the core of the fluid region ($0 < r < 0.4$), while it decreases in the remaining fluid region including the porous bed (Fig. 3a). The temperature slightly rises in the entire region with an increase in D^{-1} (Fig. 4a). In other words, the lower the permeability of the porous medium, the higher the temperature in the fluid region.

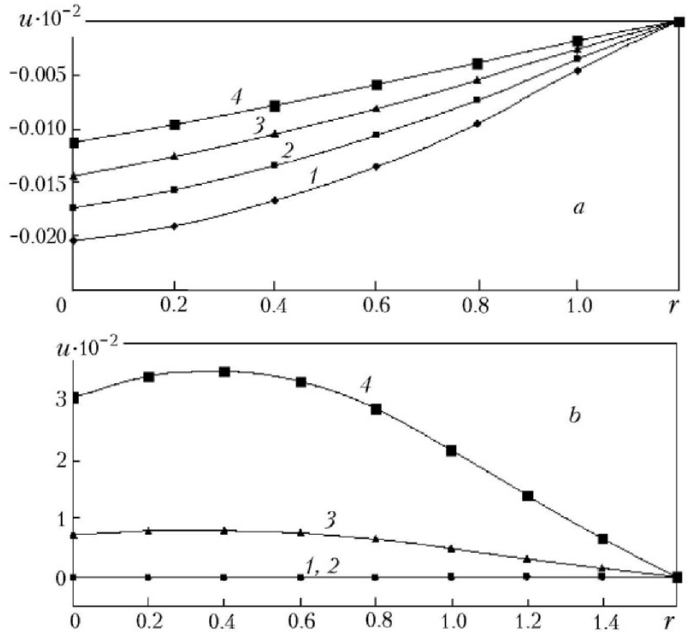

Fig. 1. Velocity profiles at $D^{-1} = 10^3$, $s = 0.2$ (a) and 0.6 (b) for different values of the Grashof number: 1) G = 50; 2) 100; 3) 150; 4) 200.

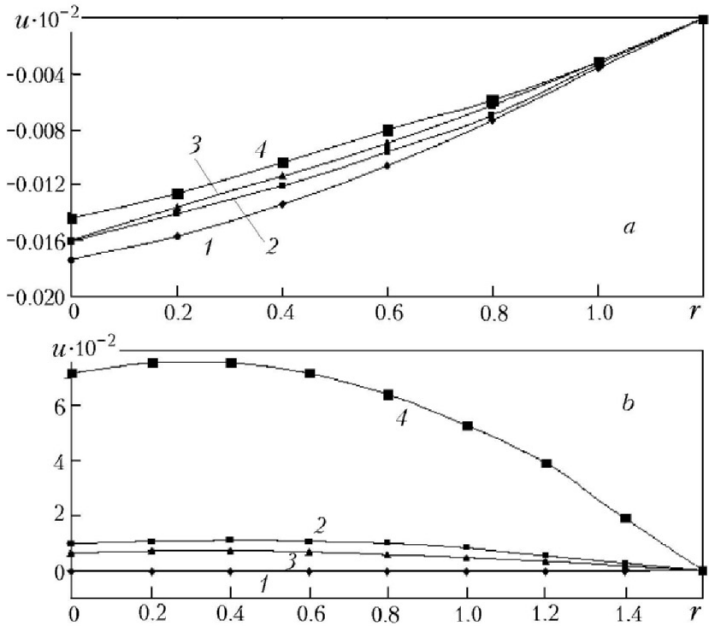

Fig. 2. Velocity profiles at G = 50, $s = 0.2$ (a) and 0.6 (b) for different values of D^{-1}: 1) $D^{-1} = 10^3$; 2) $2 \cdot 10^3$; 3) $3 \cdot 10^3$; 4) $4 \cdot 10^3$.

In the case of a porous bed of larger thickness, the temperature is almost independent of G for smaller values of G ($G \leq 10^2$), but a further increase in G enhances the temperature in all the region (Fig. 3b). The behavior of the temperature with variation in D^{-1} for large s is the same as for the velocity (Fig. 4b). Figure 5a shows the velocity profiles for different values of the thickness of the porous bed. As was pointed earlier, the fluid moves with a larger velocity when the thickness of the porous bed grows. Likewise, the temperature also increases in the entire region with the thickness (Fig. 5b).

The shear stress on the outer cylinder is evaluated for different values of the parameters and is given in Tables 1 and 2. It is seen from the tables that for smaller thickness of the porous bed an increase in G reduces the shear

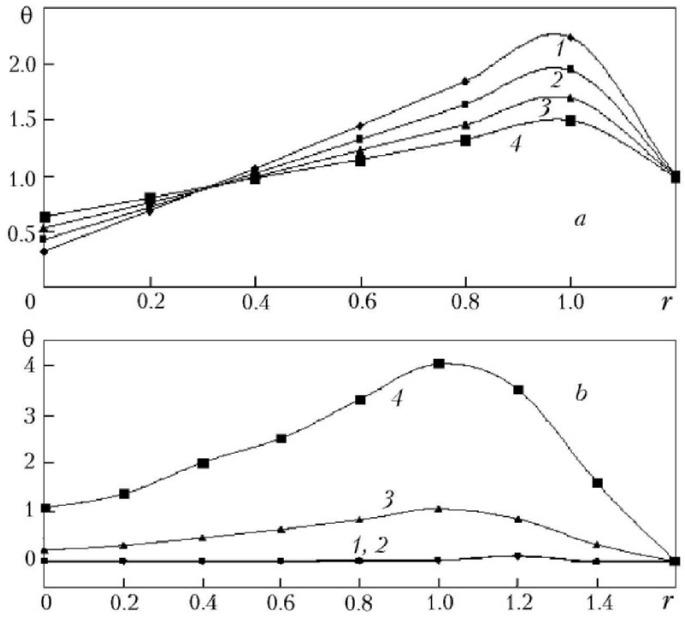

Fig. 3. Temperature profiles at $D^{-1} = 10^3$, $s = 0.2$ (a) and 0.6 (b) for different values of the Grashof number: 1) G = 50; 2) 100; 3) 150; 4) 200.

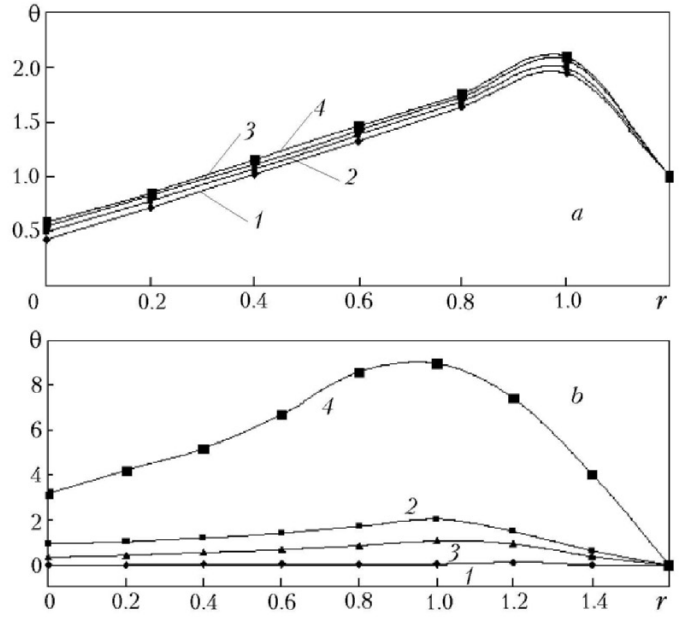

Fig. 4. Temperature profiles at G = 50, $s = 0.2$ (a) and 0.6 (b) for different values of D^{-1}: 1) $D^{-1} = 10^3$; 2) $2 \cdot 10^3$; 3) $3 \cdot 10^3$; 4) $4 \cdot 10^3$.

stress. For sufficiently large thickness the shear stress is reduced with an increasing G for smaller values of G ($G \leq 10^2$), but with a further increase in G the stress becomes negative and higher in magnitude. The change in the sign of the shear stress implies the appearance of a reversal flow at higher values of G. From Table 2 we see that the shear stress increases with D^{-1} for all the thicknesses of the bed.

The rate of heat transfer for different values of s, G, and D^{-1} is also presented in Tables 1 and 2. For lower values of G an increase in G leads to a decrease in the Nusselt number, but when G is large, Nu increases with G. We also notice that the larger the thickness of the bed, the lower is the rate of heat transfer for all values of G and

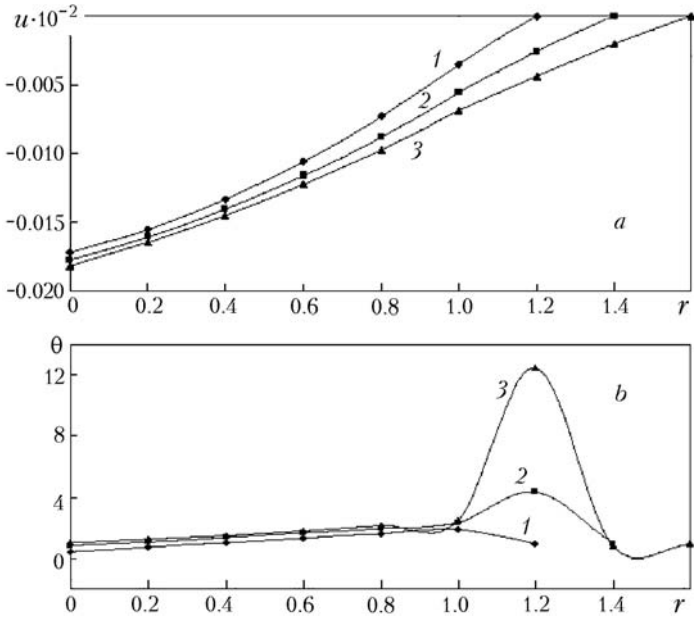

Fig. 5. Velocity (a) and temperature (b) profiles at G = 50, $D^{-1} = 10^3$ for different values of s: 1) s = = 0.2; 2) 0.4; 3) 0.6.

TABLE 1. Shear Stress and Nusselt Number on Outer Cylinder for $D^{-1} = 10^3$ and Different Values of G and s

s	G					
	50		100		150	
	τ	Nu	τ	Nu	τ	Nu
0.4	1.9219	79.2557	1.2889	78.0147	0.8620	137.0802
0.5	1.6071	63.8268	1.1294	62.664	–76.7714	129.097
0.6	1.5284	53.5265	1.0526	52.3946	–57.4586	88.6656

TABLE 2. Shear Stress and Nusselt Number on Outer Cylinder for G = 50 and Different Values of D^{-1} and s

s	$D^{-1} \cdot 10^{-3}$					
	1		2		3	
	τ	Nu	τ	Nu	τ	Nu
0.4	1.8323	79.6192	1.9545	80.0218	2.0906	80.47
0.5	1.7688	64.3529	1.9588	64.9709	2.1853	65.7072
0.6	1.7552	54.2558	2.0441	55.1831	2.4173	56.3791

D^{-1}. We conclude also that the lower the permeability of the medium, the higher the rate of heat transfer for all the values of s and G.

NOTATION

a, duct radius; A, temperature gradient; c_p, specific heat at a constant pressure; D^{-1}, inverse Darcy parameter; F, function dependent on the Reynolds number and microstructure of the porous medium; g, acceleration of gravity; G, Grashof number; k, permeability; N, nondimensional temperature gradient; Nu, Nusselt number; p, pressure; Pr, Prandtl number; r, radial coordinate; s, width of the porous bed; T, temperature; u, velocity component in the axial direction; z, axial coordinate; β, coefficient of thermal expansion; γ, kinematic viscosity; δ, porosity; λ, thermal conductivity; Λ, inertia parameter; μ, viscosity; θ, nondimensional temperature; ρ, density; τ, shear stress. Subscripts: p, porous bed; 0, equilibrium value; 1, outer boundary.

REFERENCES

1. G. S. Beavers and D. D. Joseph, Boundary conditions at a naturally permeable wall, *J. Fluid Mech*., **13**, 197–207 (1967).
2. K. Vafai and R. Thiyagaraja, Analysis of flow and heat transfer at the interface region of a porous medium, *Int. J. Heat Mass Transfer*, **30**, 1391–1405 (1987).
3. K. Vafai and S. J. Kim, Fluid mechanics of the interface region between a porous medium and a fluid layer — an exact solution, *Int. J. Heat Mass Transfer*, **11**, 254–256 (1990).
4. D. Poulikakos and M. Kazmierczak, Forced convection in a duct partially filled with a porous material, *J. Heat Transfer*, **109**, 653–662 (1987).
5. J. Y. Jang and J. L. Chen, Forced convection in a parallel plate channel partially filled with a high-porosity medium, *Int. Comm. Heat Mass Transfer*, **19**, 263–273 (1992).
6. K. Vafai and S. J. Kim, On the limitations of the Brinckman–Forchheimer–extended Darcy equation, *Int. J. Heat Fluid Flow*, **16**, 11–15 (1995).